Research Article

Vol. 24, No. 18 | 5 Sep 2016 | OPTICS EXPRESS 20973

Optics EXPRESS

Quantum detector tomography of a single-photon frequency upconversion detection system

JIANHUI MA,[1] XIULIANG CHEN,[1] HUIQIN HU,[1] HAIFENG PAN,[1] E WU,[1,2,*] AND HEPING ZENG[1]

[1]*State Key Laboratory of Precision Spectroscopy, East China Normal University, No. 3663 Zhongshan North Road, Shanghai 200062, China*

[2]*Collaborative Innovation Center of Extreme Optics, Shanxi University, Taiyuan, Shanxi 030006, China*

[*]*ewu@phy.ecnu.edu.cn*

Abstract: We experimentally presented a full quantum detector tomography of a synchronously pumped infrared single-photon frequency upconversion detector. A maximum detection efficiency of 37.6% was achieved at the telecom wavelength of 1558 nm with a background noise about 1.0×10^{-3} counts/pulse. The corresponding internal quantum conversion efficiency reached as high as 84.4%. The detector was then systematically characterized at different pump powers to investigate the quantum decoherence behavior. Here the reconstructed positive operator valued measure elements were equivalently illustrated with the Wigner function formalism, where the quantum feature of the detector is manifested by the presence of negative values of the Wigner function. In our experiment, pronounced negativities were attained due to the high detection efficiency and low background noise, explicitly showing the quantum feature of the detector. Such quantum detector could be useful in optical quantum state engineering, quantum information processing and communication.

OCIS codes: (190.7220) Upconversion; (270.5570) Quantum detectors; (040.3780) Low light level.

References and links

1. J. T. Gomes, L. Delage, R. Baudoin, L. Grossard, L. Bouyeron, D. Ceus, F. Reynaud, H. Herrmann, and W. Sohler, "Laboratory demonstration of spatial-coherence analysis of a blackbody through an up-conversion interferometer," Phys. Rev. Lett. **112**(14), 143904 (2014).
2. J. S. Dam, P. Tidemand-Lichtenberg, and C. Pedersen, "Room-temperature mid-infrared single-photon spectral imaging," Nat. Photonics **6**(11), 788–793 (2012).
3. K. Huang, X. Gu, H. Pan, E. Wu, and H. Zeng, "Few-photon-level two-dimensional infrared imaging by coincidence frequency upconversion," Appl. Phys. Lett. **100**(15), 151102 (2012).
4. R. E. Warburton, A. McCarthy, A. M. Wallace, S. Hernandez-Marin, R. H. Hadfield, S. W. Nam, and G. S. Buller, "Subcentimeter depth resolution using a single-photon counting time-of-flight laser ranging system at 1550 nm wavelength," Opt. Lett. **32**(15), 2266–2268 (2007).
5. J. O. Arroyo and P. Kukura, "Non-fluorescent schemes for single-molecule detection, imaging and spectroscopy," Nat. Photonics **10**(1), 11–17 (2015).
6. J. Zhang, M. A. Itzler, H. Zbinden, and J. W. Pan, "Advances in InGaAs/InP single-photon detector systems for quantum communication," Light Sci. Appl. **4**(5), e286 (2015).
7. K. Takemoto, Y. Nambu, T. Miyazawa, Y. Sakuma, T. Yamamoto, S. Yorozu, and Y. Arakawa, "Quantum key distribution over 120 km using ultrahigh purity single-photon source and superconducting single-photon detectors," Sci. Rep. **5**, 14383 (2015).
8. F. Marsili, V. B. Verma, J. A. Stern, S. Harrington, A. E. Lita, T. Gerrits, I. Vayshenker, B. Baek, M. D. Shaw, R. P. Mirin, and S. W. Nam, "Detecting single infrared photons with 93% system efficiency," Nat. Photonics **7**(3), 210–214 (2013).
9. P. Rath, O. Kahl, S. Ferrari, F. Sproll, G. Lewes-Malandrakis, D. Brink, K. Ilin, M. Siegel, C. Nebel, and W. Pernice, "Superconducting single-photon detectors integrated with diamond nanophotonic circuits," Light Sci. Appl. **4**(10), e338 (2015).
10. M. A. Albota and F. N. Wong, "Efficient single-photon counting at 1.55 microm by means of frequency upconversion," Opt. Lett. **29**(13), 1449–1451 (2004).

#272685 http://dx.doi.org/10.1364/OE.24.020973

Journal © 2016 Received 28 Jul 2016; revised 26 Aug 2016; accepted 26 Aug 2016; published 31 Aug 2016

11. C. Langrock, E. Diamanti, R. V. Roussev, Y. Yamamoto, M. M. Fejer, and H. Takesue, "Highly efficient single-photon detection at communication wavelengths by use of upconversion in reverse-proton-exchanged periodically poled LiNbO3 waveguides," Opt. Lett. **30**(13), 1725–1727 (2005).
12. H. Pan, H. Dong, H. Zeng, and W. Lu, "Efficient single-photon counting at 1.55 mum by intracavity frequency upconversion in a unidirectional ring laser," Appl. Phys. Lett. **89**(19), 191108 (2006).
13. H. Dong, H. Pan, Y. Li, E. Wu, and H. Zeng, "Efficient single-photon frequency upconversion at 1.06 mum with ultralow background counts," Appl. Phys. Lett. **93**(7), 071101 (2008).
14. Y. Iwai, T. Honjo, K. Inoue, H. Kamada, Y. Nishida, O. Tadanaga, and M. Asobe, "Polarization-independent, differential-phase-shift, quantum-key distribution system using upconversion detectors," Opt. Lett. **34**(10), 1606–1608 (2009).
15. P. S. Kuo, O. Slattery, Y. S. Kim, J. S. Pelc, M. M. Fejer, and X. Tang, "Spectral response of an upconversion detector and spectrometer," Opt. Express **21**(19), 22523–22531 (2013).
16. M. Legré, R. Thew, H. Zbinden, and N. Gisin, "High resolution optical time domain reflectometer based on 1.55mum up-conversion photon-counting module," Opt. Express **15**(13), 8237–8242 (2007).
17. E. Pomarico, B. Sanguinetti, R. Thew, and H. Zbinden, "Room temperature photon number resolving detector for infared wavelengths," Opt. Express **18**(10), 10750–10759 (2010).
18. K. Huang, X. Gu, M. Ren, Y. Jian, H. Pan, G. Wu, E. Wu, and H. Zeng, "Photon-number-resolving detection at 1.04 μm via coincidence frequency upconversion," Opt. Lett. **36**(9), 1722–1724 (2011).
19. G. Temporão, S. Tanzilli, H. Zbinden, N. Gisin, T. Aellen, M. Giovannini, and J. Faist, "Mid-infrared single-photon counting," Opt. Lett. **31**(8), 1094–1096 (2006).
20. X. Gu, K. Huang, H. Pan, E. Wu, and H. Zeng, "Efficient mid-infrared single-photon frequency upconversion detection with ultra-low background counts," Laser Phys. Lett. **10**(5), 055401 (2013).
21. G. L. Shentu, X. X. Xia, Q. C. Sun, J. S. Pelc, M. M. Fejer, Q. Zhang, and J. W. Pan, "Upconversion detection near 2 μm at the single photon level," Opt. Lett. **38**(23), 4985–4987 (2013).
22. M. T. Rakher, L. Ma, O. Slattery, X. Tang, and K. Srinivasan, "Quantum transduction of telecommunications-band single photons from a quantum dot by frequency upconversion," Nat. Photonics **4**(11), 786–791 (2010).
23. C. E. Vollmer, C. Baune, A. Samblowski, T. Eberle, V. Händchen, J. Fiurášek, and R. Schnabel, "Quantum up-conversion of squeezed vacuum states from 1550 to 532 nm," Phys. Rev. Lett. **112**(7), 073602 (2014).
24. P. Kumar, "Quantum frequency conversion," Opt. Lett. **15**(24), 1476–1478 (1990).
25. R. Tang, X. Li, W. Wu, H. Pan, H. Zeng, and E. Wu, "High efficiency frequency upconversion of photons carrying orbital angular momentum for a quantum information interface," Opt. Express **23**(8), 9796–9802 (2015).
26. A. P. VanDevender and P. G. Kwiat, "Quantum transduction via frequency upconversion," J. Opt. Soc. Am. B **24**(2), 295–299 (2007).
27. X. Gu, K. Huang, H. Pan, E. Wu, and H. Zeng, "Photon correlation in single-photon frequency upconversion," Opt. Express **20**(3), 2399–2407 (2012).
28. J. S. Lundeen, A. Feito, H. Coldenstrodt-Ronge, K. L. Pregnell, Ch. Silberhorn, T. C. Ralph, J. Eisert, M. B. Plenio, and I. A. Walmsley, "Tomography of quantum detectors," Nat. Phys. **5**(1), 27–30 (2009).
29. V. D'Auria, N. Lee, T. Amri, C. Fabre, and J. Laurat, "Quantum decoherence of single-photon counters," Phys. Rev. Lett. **107**(5), 050504 (2011).
30. J. Fiurášek, "Maximum-likelihood estimation of quantum measurement," Phys. Rev. A **64**(2), 024102 (2001).
31. P. S. Kuo, J. S. Pelc, O. Slattery, Y. S. Kim, M. M. Fejer, and X. Tang, "Reducing noise in single-photon-level frequency conversion," Opt. Lett. **38**(8), 1310–1312 (2013).
32. X. Gu, K. Huang, Y. Li, H. Pan, E. Wu, and H. Zeng, "Temporal and spectral control of single-photon frequency upconversion for pulsed radiation," Appl. Phys. Lett. **96**(13), 131111 (2010).

1. Introduction

Infrared single-photon detections have been developed rapidly and extensively used for various applications in astronomy, imaging, metrology, ultrasensitive spectroscopy, quantum key distribution (QKD) and so forth [1–7]. Recent progresses in superconducting nanowire single-photon detectors attract researchers' attention because of the high detection efficiency, low dark-count noise, low timing jitter and fast response [8,9]. However, the cryostats are still required to operate the superconducting nanowire single-photon detectors. Therefore, the InGaAs/InP avalanche photodiodes (APDs) are yet the preferred choice in the infrared single-photon detection due to their compactness and convenience [6]. Recently, another efficient single-photon detection technique for the infrared, the single-photon frequency upconversion detectors (UCDs) which use Si-APDs to count the visible sum-frequency replicas of the infrared photons, has attracted more and more research interest. They have avoided the drawbacks of the InGaAs/InP APDs of low detection efficiency, large dark-count noise and large afterpulsing effect [10–13]. The UCDs have been successfully employed in the QKD, spectrum analysis, laser ranging and so on [14–16]. Infrared photon-number resolving detection and sensitive imaging have also been realized via frequency upconversion [17,18]. And this method has been extended to the longer wavelengths, leading to the sensitive detection of mid-infrared signals at single-photon level [19–21]. Especially, the UCDs have been implemented to the detection of different quantum states [22,23]. Quantum detector tomography (QDT) of the Si-SPCM for the single-photon detection at visible regime has been demonstrated to characterize the detector's performance in the quantum state detection with no ancillary assumptions. However, the UCD as a special kind of infrared single-photon detector could not be simply regarded the same as a Si-SPCM detecting at a different wavelength because of the intrinsic pump-power related detection efficiency and parametric fluorescence noise. Therefore, characterizing the UCD by QDT would help to understand the quantum capability of such infrared single-photon detectors and for the applications in quantum information processing.

In this paper, we experimentally demonstrated and characterized an infrared UCD system by QDT. The UCD was based on a synchronously pumped sum-frequency generation (SFG) system. The signal photons at 1558 nm were converted to 622 nm in a periodically poled lithium niobate (PPLN) bulk crystal with the highest conversion efficiency of 84.4% and detected by a Si-APD single-photon detector. The total detection efficiency of the UCD was about 37.6% with a background noise of 1.0×10^{-3} counts/pulse. The positive operator valued measure (POVM) of this infrared single-photon detection device was obtained by the quantum detector tomography. From the POVM elements, the corresponding Wigner functions at different detection efficiencies were established, revealing the quantum feature of the detector. This study shows that the UCD is fundamentally a quantum detector despite of the existence of the parametric fluorescent noise.

The UCD is based on the three-wave mixing SFG process where the wavelength of the signal photons is translated to shorter regime with the preservation of all the quantum characteristics. In the UCD system, the pump field is typically strong with negligible depletion. Therefore, the pump field can be treated classically as a constant E_p, leading to an interaction Hamiltonian as [24]

$$\hat{H} = i\hbar g E_p (\hat{a}_1 \hat{a}_2^+ - H.c), \tag{1}$$

where $\hat{a}_1$ is the annihilation operator of the signal photons at ω_1, $\hat{a}_2^+$ is the creation operator corresponding to the upconverted photons at ω_2, g is the coupling constant determined by the second-order susceptibility of the nonlinear medium, and $H.c.$ denotes a Hermitian conjugate. The conversion efficiency is dependent on the pump field intensity as

$$\eta = \sin^2(|gE_p|L), \tag{2}$$

where L is the length of the nonlinear crystal. To achieve the unity conversion efficiency, a strong laser field in a long quadratic nonlinear medium with a large effective nonlinear coefficient is required by the UCD to fulfill

$$|gE_p|L = \pi/2 \tag{3}$$

2. Experiment setup

We designed and demonstrated a synchronously pumped infrared single-photon frequency upconversion detector with high efficiency and low noise. The experimental setup of the UCD as shown in Fig. 1 consisted of three parts. The signal and pump sources part included two synchronized mode-locked fiber lasers and the corresponding amplifiers. The two fiber lasers were synchronized in master-slave configuration with repetition rate of 20.3 MHz [25]. The master laser was an erbium-doped fiber laser (EDFL) which was passively mode-locked by nonlinear polarization rotation effect in the fiber cavity. A part of the output from the EDFL was filtered by a fiber Bragg grating (FBG) to fulfill the acceptance bandwidth of the

PPLN crystal. The spectral bandwidth of the signal was 0.5 nm with the central wavelength at 1558.0 nm, and the pulse duration was measured to be 12.4 ps. The laser pulses was attenuated to few-photon level to be used as the signal photons. The other part of the EDFL output was amplified and injected into the slave laser to trigger the mode-locking by the cross-phase modulation induced by the nonlinear polarization rotation, which was an ytterbium-doped fiber laser (YDFL). The spectrum of the YDFL was also filtered by a FBG at 1036.0 nm with bandwidth of 0.3 nm to be used as the pump for the frequency upconversion. The pump laser could provide a maximum average power of 100 mW by a two-stage amplification. The pulse duration of the pump source was 31.4 ps so that the corresponding signal photons could be wholly enveloped in the pump pulse. And accordingly, the peak power of the pump laser was calculated to be 160 W, providing the strong undepleted pump field. Thanks to the synchronously pumping scheme, a high conversion efficiency could be achieved easily since the pulse duration of the power laser was so short that the peak power of the pump pulse could fulfill the complete conversion requirement. By engineering the structures and intracavity dispersion-management of the two fiber lasers, the YDFL and followed fiber amplifier generated pump pulses of a little longer pulse duration than the EDFL signal. The single-photon signal could be synchronously gated within the pump pulse, so each single photon could interact with the corresponding pump pulse in the PPLN crystal to guarantee an efficient frequency upconversion and high detection efficiency.

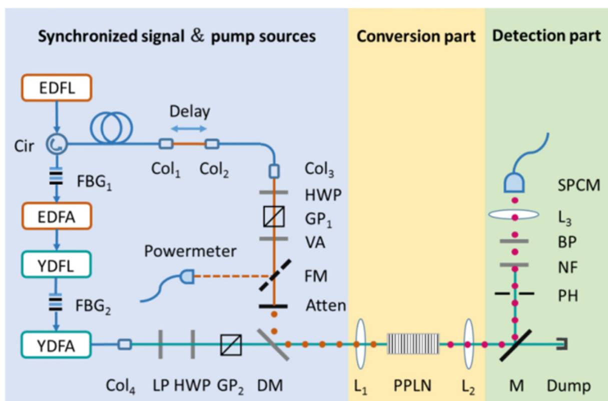

Fig. 1. Schematic of the experimental setup. EDFL: erbium-doped fiber laser; YDFL: ytterbium-doped fiber laser; EDFA: erbium-doped fiber amplifier; YDFA: ytterbium-doped fiber amplifier; Cir: circulator; $Col_{1,2,3,4}$: collimators; Atten: fixed attenuator; FBG_1: fiber Bragg grating at 1558 nm; FBG_2: fiber Bragg grating at 1036 nm; LP: long-pass filter cutting off at 1000 nm; BP: band-pass filter at 622 nm; HWP: half wave plate; $GP_{1,2}$: Glan prisms; FM: flip mirror; VA: variable attenuator; DM: dichroic mirror; $L_{1,2,3}$: lenses; PPLN: periodically poled lithium niobate; M: mirror with high reflectivity at 622 nm; PH: pinhole; NF: notch filter; SPCM: single-photon counting module.

In the frequency upconversion part, the signal beam and the pump beam were combined in a PPLN bulk crystal by a dichroic mirror which reflected the signal photons at 1558 nm and transmitted the pump beam at 1036 nm. Before focused to the PPLN crystal, the two beams were both adjusted to be vertically linear-polarized by the half-wave plates and the Glan prisms. And a long-pass filter cutting off at 1000 nm was inserted in the pump beam to stop the noise photons from the optical fiber. The combined beams were focused to the center of PPLN crystal by an achromatic lens. The PPLN crystal in our experiment was 50 mm in length, offering a long interaction length for the signal photons and the pump pulses. The inverse period of the PPLN was 11.0 μm, and the temperature of the PPLN crystal was controlled at 119 °C to fulfill the quasi-phase matching condition. The signal photons would be translated to the SFG wavelength in the PPLN crystal when they overlapped with the

Optics EXPRESS

pump pulse in time and space. Because the two facets of the PPLN bulk crystal were antireflection coated for signal, pump and converted signal, the coupling efficiency of the PPLN bulk crystal was higher than that of the PPLN waveguide. As a result, the detection efficiency of UCD using the PPLN crystal would be higher than using waveguide with the same conversion efficiency.

In the detection part, the SFG output beam was steered to pass through the spectral filters before entering the Si-APD single-photon counting module (SPCM), including a high reflection mirror at 622 nm and anti-reflection at 1036 nm, a notch filter at 1036 nm, and a band-pass filter at 622 nm. The total transmittance of the filters for the SFG photons was about 71.8%. The SFG beam was focused to the SPCM. The detection efficiency of the SPCM (SPCM-AQ-RH-14, Excelitas Technologies Corp.) was 62% around 620 nm and the maximum counting rate was 43.7 MHz, which was higher than the repetition rate of the laser sources. The whole detection part was placed in a dark box with a small aperture for the incident SFG photons in order to shield the system from the environment noise. The background noise of the UCD was about 300 counts/s with the aperture open and the pump source off, which included darkcount noise of the SPCM itself of 150 counts/s. Since this background noise distributed randomly in time domain, considering the low duty cycle ratio of the system, it could be ignored comparing with the parametric fluorescence noise from the strong pump which was located within the same pump pulse as the SFG photons.

3. Results

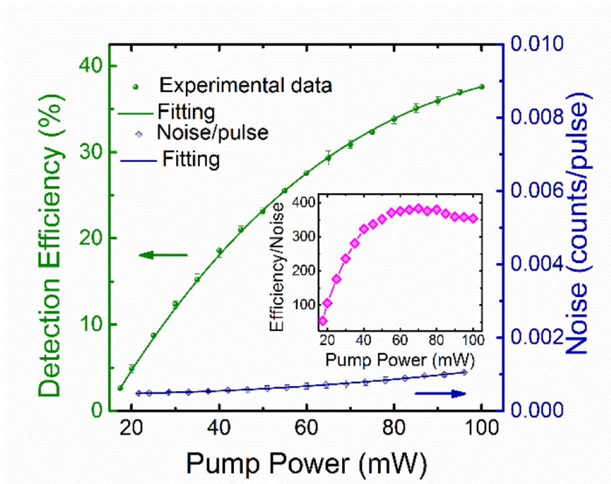

Fig. 2. Detection efficiency and background noise as a function of the pump power. Inset: Efficiency to noise ratio dependent on the pump power. The error bars are produced from the standard deviation of repeated experiment measurements.

Keeping the signal photon intensity at about 0.1 photon/pulse, we varied the pump power from 10 mW to 100 mW, and the detection efficiency as well as the background noise was recorded as a function of the pump power as shown in Fig. 2. The fitting of the detection efficiency is according to

$$\eta_D = T_f \eta_Q \sin^2(\frac{\pi}{2}\sqrt{\frac{P_{pump} - P_0}{P_{sat}}}), \tag{4}$$

where T_f is the transmittance of the filtering system for SFG including two lenses, a dichroic mirror with high reflectivity at 622 nm, an iris, a notch filter, and a bandpass filter, η_Q stands for the quantum efficiency of the Si-SPCM, P_{pump} is the incident pump power, P_0 is the offset

Optics EXPRESS

for the unexpected loss of the pump power, and P_{sat} is the net pump power entering the PPLN when conversion efficiency reached 100% theoretically. The error bars are produced from the standard deviation of repeated experiment measurements. With the increase of the pump power, the detection efficiency increased rapidly at the beginning but tended to be saturated when the pump power got high. With the maximum pump power of 100 mW, the detection efficiency reached 37.6%, corresponding to a conversion efficiency of 84.4% taking into account the transmittance of the filtering system and the detection efficiency of the SPCM. As shown by the fitting curve in Fig. 2, the complete quantum conversion would appear when the pump power increased to 112 mW, meaning that if the pump power further increased the periodical oscillation of the conversion efficiency dependent on the pump field intensity would appear as predicted according to Eq. (2) [26,27]. Meanwhile, the parametric fluorescence noise caused by the strong pump beam in the PPLN crystal increased nonlinearly. Considering the pulsed pump mode, the noise was localized within a very short pump time window which was much shorter than any electronic gates applied on the APD, leading to a very low noise counts on the detector. Therefore, the efficiency-noise ratio reached a maximum at the pump power of 70 mW and dropped a little at higher pump powers. To evaluate the effect of the parametric fluorescence noise on the quantum detection performance, we carried out the quantum detector tomography of this UCD system.

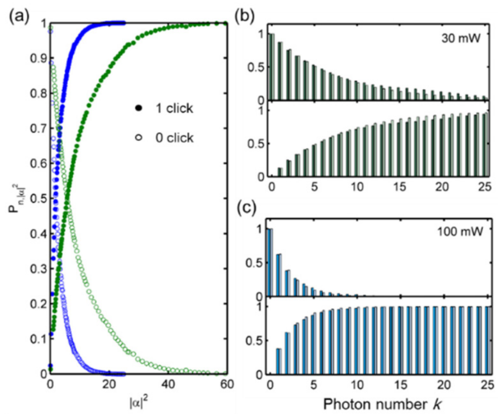

Fig. 3. Detection probability and the POVMs at different pump powers. (a) Detection probability at different pump powers of 30 mW and 100 mW, respectively. Green points: at pump power of 30 mW; blue points: at pump power of 100 mW. $|\alpha|^2$ denotes the average photon number per pulse of the signal states. (b) $\hat{\Pi}_{off}$ and $\hat{\Pi}_{on}$ at the pump power of 30 mW. (c) $\hat{\Pi}_{off}$ and $\hat{\Pi}_{on}$ at the pump power of 100 mW. Dark color bars: reconstructed POVM based on QDT; light color bars: simulated POVMs based on experimental measured η and ν.

To fully characterize this UCD, we demonstrated the QDT at different pump powers of 30 and 100 mW, respectively. For the QDT, the coherent state photon source could be used as a probe to form a complete basis [28,29]. In the experiment, the signal photons were from the attenuated laser source. At each pump power, the incident signal photon intensity was changed from 0 to 60 photons/pulse by a variable attenuator (VA) together with a fixed attenuator (Atten: −13.7 dB, −18 dB, −28.6 dB, and −35.9 dB for alternations) in the signal beam, while the counting rate of the SPCM was recorded. In order to monitor the incident photon intensity, a powermeter was inserted between VA and Atten to measure the intensity every time we tuned VA. The attenuation of the fixed attenuators was calibrated separately with a continuous-wave diode laser at the same wavelength. Since the SPCM was used in the system, the UCD could be regarded as an on/off detector, which means that the outcome of the detection is registered as either 1 click or 0 clicks. Figure 3(a) shows the detection probabilities for 1 click and 0 clicks at different pump powers. Green points indicate the detection probability at pump power of 30 mW and blue points correspond to the detection probability at pump power of 100 mW. Meanwhile the solid points and the hollow points show the cases for 1 click and 0 clicks, respectively. The curve consisting of blue solid points ascents faster than the curve consisting of green solid points, indicating that the UCD has higher detection efficiency at pump power of 100 mW than at pump power of 30 mW. As an "on/off" photon counter, the UCDs could be assumed as a phase-insensitive detector. The POVM elements thus contain only diagonal entries

$$\hat{\Pi}_n = \sum_{k=0}^{M} r_{k,n} \left|k\right\rangle\left\langle k\right|, \tag{5}$$

where the $r_{k,n}$ of POVM density matrices $\hat{\Pi}_{on}$ and $\hat{\Pi}_{off}$ are reconstructed by using the maximum likelihood algorism [30] as shown by the dark color bars in Fig. 3(b) and 3(c).

For an ideal perfect single-photon detector, one can get "0" output only with an incident vacuum state. Any other input states will result in the output of "1". Therefore, a perfect on/off detector can be described by two POVM elements as $\hat{\Pi}_{off} = \left|0\right\rangle\left\langle 0\right|$ and $\hat{\Pi}_{on} = \mathbf{1} - \left|0\right\rangle\left\langle 0\right|$ [30]. In practice, a UCD always has a limited total detection efficiency and nonnegligible background noise. Moreover, both the total detection efficiency and the background noise caused by the parametric fluorescence are dependent on the pump power. Accordingly, the general POVM elements for the UCD can be modified as

$$\hat{\Pi}_{off} = e^{-\nu(P)} \sum_{k=0}^{\infty} [1-\eta(P)]^k \left|k\right\rangle\left\langle k\right|, \qquad \hat{\Pi}_{on} + \hat{\Pi}_{off} = \mathbf{1}, \tag{6}$$

where $\eta(P)$ stands for the total detection efficiency, and $\upsilon(P)$ is the average noise photon number per pulse. Both $\eta(P)$ and $\upsilon(P)$ are related to the pump power. The POVM elements based on the experimental measured η and υ could be simulated as light color bars in Fig. 3(b) and 3(c). The reconstructed operators $\hat{\Pi}_{on}$ and $\hat{\Pi}_{off}$ based on QDT and simulated POVMs based on experimental measured η and v agreed with each other quite well at different pump powers. That proved the uniformity of measurement by the two methods. Compared with our previous work with similar configuration [25], the maximum conversion efficiency was improved a little to 84.4%, and overall detection efficiency increased to 37.6%.

The Wigner function of the POVM elements is usually used to visualize the quantum features of the single-photon detector. The general Wigner function of $\hat{\Pi}_{off}$ could be written as [30]

$$W_{off}(x, y) = \sum_{k=0}^{M} r_{k,off} W_k(x+y), \tag{7}$$

where M is the truncated photon number used in the reconstruction of POVM, and W_k is the Wigner function of Fock state $\left|k\right\rangle$. Since $\hat{\Pi}_{on} + \hat{\Pi}_{off} = \mathbf{1}$, the Wigner function for $\hat{\Pi}_{on}$ can be written as

$$W_{on}(x, y) = W_1(x, y) - W_{off}(x, y). \tag{8}$$

As the UCD is considered as a phase-insensitive detector, the Wigner function is rotationally symmetric around the origin. Hence, the cross section of $W_{on}(x, 0)$ is usually plotted to represent the whole Wigner function. Figure 4(a) shows in solid lines the cross sections of Wigner function obtained by the reconstructed POVM at different pump powers of 30 and 100 mW, respectively. The $2\pi\sigma_0 W_{on}(0, 0)$ was −0.027 and −0.105, respectively. The negative values of the Wigner function at the origin of coordinate indicate this UCD is

Optics EXPRESS

fundamentally a quantum detector due to its high detection efficiency and low background noise.

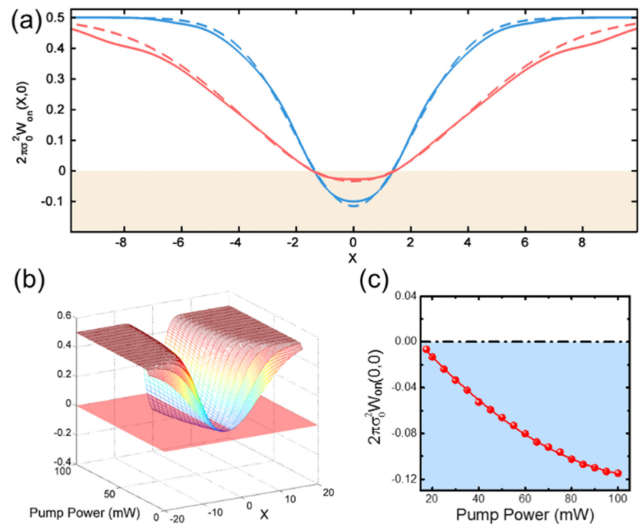

Fig. 4. Wigner function of the UCD. (a) Cross sections of the Wigner function of the UCD at pump powers of 30 mW (solid red line) and 100 mW (solid blue line) with the simulations (dashed lines). (b) Evolution of the Wigner function cross section curves. (c) $2\pi\sigma_0^2 W_{on}(0,0)$ values as a function of the pump power.

With the theoretical simulated POVM, the Wigner function for $\hat{\Pi}_{on}$ can be represented as a function of the detection efficiency and the background noise

$$W_{on} = \frac{1}{2\pi\sigma_0^2}[\frac{1}{2} - \frac{e^{-\nu(P)}}{2-\eta(P)} e^{-(x^2+y^2)/2\sigma_\eta^2}], \tag{9}$$

where

$$\sigma_\eta = \frac{2\text{-}\eta}{\eta}\sigma_0. \tag{10}$$

Without loss of generality, we can set $\sigma_0 = 1$.

As shown in Fig. 4(a), the simulated Wigner function curves in dashed lines exhibit high similarity to the one obtained from the reconstructed POVM. Therefore, we simulated the Wigner functions for all the data points of Fig. 2 to demonstrate the evolution of the quantum coherence of the UCD system. In the simulation, the noise of the system is taken into account according to Eq. (6) by the term $e^{-\nu(P)}$. According to Eq. (9), if the noise increases with the pump power while the detection efficiency is the same, the $W_{on}(x, 0)$ will rise from negative values to zero till $\nu(P)\sim\eta/2$, and the quantum coherence of the detector will disappear [29]. However, as the pump power increases, the detection efficiency of the UCD increases as well, and a high detection efficiency helps to keep the quantum coherence of the detector. In Fig. 4(b), the $W_{on}(x, 0)$ curves are plotted according to the pump power. All the values at the origin of coordinate are below zero, and the evolution of the negative dip could be observed clearly. As shown in Fig. 4(c), when the detection efficiency is below 10%, the $W_{on}(0, 0)$ for the UCD is very close to zero because the noise of the system is high but the detection efficiency is low. With the pump power increasing, the negative dip of $W_{on}(0, 0)$ at the origin drops deeper and deeper. In this synchronous pumping system, although the background noise increased nonlinearly with the pump power, $W_{on}(0, 0)$ is far below zero even at the maximum pump power of 100 mW, indicating that the parametric fluorescence noise produced by the strong pump field in the PPLN crystal doesn't destroy the quantum coherence of the UCD.

4. Summary

In conclusion, we demonstrated the QDT of the UCD system in the synchronous pumping scheme. The POVMs were reconstructed from the QDT measurement, and the Wigner function curves deduced from the reconstructed POVM shows negative values at the origin, indicating the quantum coherence of the detector is not destroyed by the parametric fluorescence noise induced by the strong pump field and the UCD is fundamentally a quantum detector. If long-wavelength pumping scheme is applied in the UCD to suppress the parametric fluorescence noise [31,32], the UCD system would be more robust for the quantum state detection.

Funding

National Natural Science Fund of China (NSFC) (11621404, 61127014, 61378033, 11674099); National Key Scientific Instrument Project (2012YQ150092); Program of Introducing Talents of Discipline to Universities (B12024); Shuguang Program (15SG22); Shanghai International Cooperation Project (16520710600) .

Acknowledgments

The authors thank J. Laurat and K. Huang for discussions and suggestions.